

Dear Editor

We have addressed the reviewers' comments in the revised manuscript; our detailed responses to their comments are given below (reviewer's comments in italics). A version of the manuscript with tracked changes in red is attached below.

## **Reviewer 2**

### **General Comments:**

*This paper describes a new version of the Reading Intermediate Global Circulation Model, version 4 (IGCM4). It goes over new additions, setups, and parameterizations to the model, and examines how well the model simulates basic tropospheric and stratospheric variables, including tropospheric and stratospheric temperatures, precipitation, Outgoing Longwave Radiation (OLR), and zonally-averaged stratospheric winds. The climate sensitivity of the model coupled to a slab ocean was also examined. In general, the model does a decent job in simulating temperature, precipitation, and OLR compared to the NCEP-DOE reanalysis and CMIP5 models, with most of the errors being attributed to a lack of aerosol forcing and cloud parameterization errors. The model also compares well to ERA-40 reanalysis in the stratosphere, with errors in zonal average wind speed attributed to the model's gravity wave drag scheme.*

*I have personally never used this model. However, I think this description is easy enough to understand, and thus good enough to be accepted with revisions. The revisions I have for the paper are listed in the next two sections.*

We thank the reviewer for this positive review.

### **Specific Comments:**

There were several scientific clarifications I think would be helpful for this paper:

*1) In the introduction, it would be useful to describe the scientific benefits of having an intermediate complexity climate model. For example, it would help if you described in more detail how a "hierarchy of models" can help deduce underlying physical processes. You should also emphasize that given this model's relative computational cheapness, it would be a great candidate for running a large ensemble, or for doing very long simulations. Those long simulations themselves could help estimate equilibrium climate sensitivity given long time-scale changes and feedbacks, and could also help paleoclimate simulations. Describing these sorts of scientific benefits in the introduction would certainly strengthen this paper.*

This is a good point: we now include a section in the revised manuscript (lines 48-70) in which we include just such a rationale for the use of intermediate complexity models such as the IGCM4:

'The rationale for such a model in the hierarchy of potential model codes is now addressed. Understanding key scientific questions related to climate and climate changes relies on understanding processes within the atmosphere, whose complex and nonlinear nature entails the use of global circulation models. However, understanding such complex processes in models is extremely challenging since unpicking processes within state-of-the-art climate circulation models can be extremely difficult given their complexity- especially when their computational demands are taken into account, leading to limits in both integration times and data storage.'

'Having said that, it is necessary for models to be complex enough to simulate the processes that are relevant to understanding a given question of interest. This is the niche which intermediate circulation models such as the IGCM occupies. This niche

consists of models that are complex enough in terms of dynamical processes to represent a wide variety of processes from monsoonal circulations to extratropical storm tracks. However, their relative simplicity compared to state-of-the-art climate models that are employed by the Intergovernmental Panel on Climate Change (henceforth IPCC), enable process-level understanding to become more tractable because of (a) computational speed enabling long integrations or large ensemble members, and (b) flexibility and ease of use enabling the examination of idealised scenarios. Examples where the IGCM4 might be used are e.g.; conducting integrations of idealised perturbations to boundary conditions such as sea-surface temperature, topography, or continental distributions; conducting ensembles of multi-century integrations to collect robust statistics of small-amplitude responses to particular forcings”.

*2) In section 2.3, there is the statement “the height at which total albedo reaches (A+S)/2”. I am not sure what “height” that statement is referring to. Is that the model vertical level (e.g., one of the sigma levels), the snow depth, or something else? I think stating explicitly what that height is will help the reader.*

The value is height in metres. We now include a table which shows these surface parameters as a function of surface type (Table 1 in revised text).

*3) I am not familiar with the radiation schemes used in IGCM, and thus it is not clear what the benefit is to move from NIKOSRAD to Morcrette. Does Morcrette have ozone absorption while NIKOSRAD doesn't? Is Morcrette more physically realistic, or does it produce a more accurate climate simulation? Is it computationally cheaper, or more easily parallelized? I think spending more time describing how you chose your radiation scheme would help this document immensely.*

The NIKOSRAD scheme was found to produce  $2\Delta z$  oscillations under certain conditions in the stratosphere, which is why it was replaced. The Morcrette scheme is originally written for the ECMWF model so is fast. We now state the reason for replacing NIKOSRAD with MORCLETTE in the text.

*4) I was unable to find any description of the convective schemes used in the model, even though there are statements about tuning and rainout timescales. There needs to be a description of the convective scheme somewhere in this paper. Without one, it is impossible to have a strong opinion on the scientific validity of the model.*

We now describe the convection scheme in the IGCM4 in section 2.3 (lines 192-195): it is similar to that described in Forster et al (Clim. Dynamics, 16, 833-849, 2000).

*5) The same goes for clouds produced by the large-scale dynamics. Is there any sort of physical parameterization to deal with the radiative and microphysical effects of those? You do describe a marine stratocumulus scheme, but what about clouds over land, or those generated by extratropical cyclones that aren't convective? Again, a more complete description of the moist physics in this model is needed.*

We now describe the stratiform cloud and precipitation scheme in section 2.3 (lines 204-207); again it is identical to that described in Forster et al (Clim. Dynamics, 16, 833-849, 2000). Cyclones over both land and ocean can form stratiform cloud and precipitation.

*6) What is the dataset you are using for OLR to compare against the model? I am assuming it is NCEP-DOE reanalysis, but this isn't explicitly stated anywhere. It would be good to state in the document where you acquired your OLR data.*

We have now inserted a reference for the OLR data in the figure where it is used and in the text.

## Technical comments:

*In the last sentence of the second paragraph in section 2.3, you should drop “e.g.”, so that it just says “such as HadGEM2”.*

We have made this change.

*In the first sentence of section 2.4, you need to add the word “was”, so that the phrase is either “which was originally written” or “which originally was written”.*

We have added the word “was” to the text.

*In the first sentence of the last paragraph of section 2.4, the final wording should be changed to something like “A version of the Kawai and Inoue (2006) parameterisation for marine stratocumulus cloud has also been implemented in IGCM4.”*

We have changed the sentence to the above recommendation.

*In section 2.5, I would either drop the parenthetical phrase “a very good approximation for the stratosphere”, or add a citation to support it.*

We have dropped the phrase.

*In section 3.1, the first sentence needs the word “as” included, like so: “...is prescribed **as** a monthly-varying climatology”.*

We have made this change.

*I would probably not use the phrase “basket of models”. Maybe instead use the phrase “collection of models”, or “(sub)set of models”.*

We have changed the word “basket” to “subset”.

*In the third paragraph of section 3.1, the third sentence is somewhat difficult to read. I would reword it like so:*

*As a guide to the IGCM’s performance in the context of other models, the mean±one standard deviation precipitation bias amongst a **subset of models present in the CMIP5 archive being used** for the UN Intergovernmental Panel on Climate Change’s 5th assessment report (IPCC AR5) is also shown: the comparison is for the CMIP5 model configuration using prescribed “AMIP” SSTs, since coupled ocean-atmosphere biases tend to worsen model performance.*

We have made this change.

*I also found the third sentence of the fourth paragraph of section 3.1 difficult to understand at first. I would probably rephrase the beginning like so: “**Thus**, for the JJA season as **well as** the DJF season...”.*

We have made this change.

*In the last sentence of paragraph 5 of section 3.1, I think you meant to state that the imbalance, not the balance, of the energy fluxes is 1-2 w/m2.*

We have made this change.

*In section 4, is the climate sensitivity the equilibrium or transient sensitivity? Just specifying which type will help.*

We now specify that we mean equilibrium climate sensitivity.

*When discussing Figure 11, it might be better to call it the energy imbalance, or just the net downward energy flux.*

We have changed the wording to “imbalance”.

*In Figure 2, it may be better if there was a labeled color bar instead of labeled contours, as the actual contour values can be hard to read. However, this is more of personal opinion than a strong suggestion.*

We have added bolder and larger labels on the curves, and changed colours, to help readability.

*In Figures 4 and 5, the observed precipitation panel plot should have a different, explicitly labeled color bar. That way it doesn't make the reader think there is negative precipitation, which is unphysical. It also should state that the bottom three (CMIP5) plots are for average precipitation bias, not average precipitation.*

We have inserted a new caption to clarify these issues. It specifically mentions that there are two colour bars (a,b and c,d,e,f) and also states the CMIP5 subfigures are differences with CMAP (which is also indicated in the subfigure heading).

*Figures 7, 8 and 9 would probably be improved by adding a difference plot between the reanalysis and IGCM4. However, it isn't a must-have.*

As well as showing reanalysis, Figures 7 and 8 now overlay contours of IGCM zonal wind and temperature on colours of IGCM4-reanalysis difference to help to show where the differences are (e.g. in the southern hemisphere tropospheric jetstream). We have not done so for Figure 9, since the additional land-ocean boundary would make such a contour plot more difficult to read- rather we now show eddy fields of both IGCM4 configurations and reanalysis at both 500 hPa and 200 hPa.

*In Figure 11, I would again call it an energy imbalance, or just the net downward energy flux.*

We have changed the caption to say "Annually averaged net downward zonal surface energy imbalance"

-----

1 | **IGCM4: A fast, parallel and flexible intermediate climate model**

2

3 | M. Joshi<sup>1,2</sup>, M. Stringer<sup>3</sup>, K. van der Wiel<sup>1,2</sup>, A. O' Callaghan<sup>1,2</sup>, S. Fueglistaler<sup>4</sup>

4 | <sup>1</sup>Centre for Ocean and Atmospheric Sciences, University of East Anglia, U. K.

5 | <sup>2</sup>School of Environmental Sciences, University of East Anglia, U. K.

6 | <sup>3</sup>National Centres for Atmospheric Science, U. K.

7 | <sup>4</sup>[Department of Geosciences/Program in Atmosphere and Ocean Science](#), Princeton  
8 | University, U. S. A.

9

10 | Correspondence address:

11 | Dr. Manoj Joshi

12 | Centre for Ocean and Atmospheric Sciences

13 | School of Environmental Sciences

14 | University of East Anglia

15 | Norwich Research Park

16 | Norwich NR4 7TJ

17

18 | Email address:

19 | m.joshi@uea.ac.uk

20

21 | Submitted to Geoscientific Model Development

22

23 **Abstract**

24 The IGCM4 (Intermediate Global Circulation Model version 4) is a global spectral  
25 primitive equation climate model whose predecessors have extensively been used in  
26 areas such as climate research, process modelling, and atmospheric dynamics. The  
27 IGCM4's niche and utility lies in its speed and flexibility allied with the complexity  
28 of a primitive equation climate model. Moist processes such as clouds, evaporation,  
29 atmospheric radiation and soil moisture are simulated in the model, though in a  
30 simplified manner compared to state-of-the-art GCMs. IGCM4 is a parallelised model,  
31 enabling both very long integrations to be conducted, and the effects of higher  
32 resolutions to be explored. It has also undergone changes such as alterations to the  
33 cloud and surface processes, and the addition of gravity wave drag. These changes  
34 have resulted in a significant improvement to the IGCM's representation of the mean  
35 climate as well as its representation of stratospheric processes such as sudden  
36 stratospheric warmings. The IGCM4's physical changes and climatology are  
37 described in this paper.

## 38 1. Introduction

39 In order to better understand the physical processes that underpin climate and climate  
40 change, it is necessary to examine not only state-of-the-art climate models, but also  
41 simpler models which can have fewer degrees of freedom. In such a manner,  
42 commonly referred to as the hierarchy of models approach, a more robust picture of  
43 the causative mechanisms underlying climate processes can emerge. This paper  
44 describes the IGCM4 (Intermediate General Circulation Model 4), which is the latest  
45 incarnation of a collection of simplified climate models, collectively and usually  
46 referred to as ‘Reading IGCM’ models, after the institution where much of their  
47 development has taken place.

48 The rationale for such a model in the hierarchy of potential model codes is now  
49 addressed. Understanding key scientific questions related to climate and climate  
50 changes relies on understanding processes within the atmosphere, whose complex and  
51 nonlinear nature entails the use of global circulation models. However, understanding  
52 such complex processes in models is extremely challenging since unpicking processes  
53 within state-of-the-art climate circulation models can be extremely difficult given  
54 their complexity- especially when their computational demands are taken into account,  
55 leading to limits in both integration times and data storage.

56 Having said that, it is necessary for models to be complex enough to simulate the  
57 processes that are relevant to understanding a given question of interest. This is the  
58 niche which intermediate circulation models such as the IGCM occupies. This niche  
59 consists of models that are complex enough in terms of dynamical processes to  
60 represent a wide variety of processes from monsoonal circulations to extratropical  
61 storm tracks. However, their relative simplicity compared to state-of-the-art climate  
62 models that are employed by the Intergovernmental Panel on Climate Change

63 (henceforth IPCC), enable process-level understanding to become more tractable  
64 because of (a) computational speed enabling long integrations or large ensemble  
65 members, and (b) flexibility and ease of use enabling the examination of idealised  
66 scenarios. Examples where the IGCM4 might be used are e.g.; conducting  
67 integrations of idealised perturbations to boundary conditions such as sea-surface  
68 temperature, topography, or continental distributions; conducting ensembles of multi-  
69 century integrations to collect robust statistics of small-amplitude responses to  
70 particular forcings.

71 The base model which IGCM4 will be compared with is the so-called IGCM3 (Forster  
72 et al. 2000). The model has had many incremental updates since IGCM3, but since  
73 that was the last documented model and climatology, all improvements to IGCM4 are  
74 described with respect to IGCM3.

75 The IGCM has a number of configurations which are briefly described here in order  
76 to clarify where IGCM4 sits in relation to the others. IGCM1 is a spectral primitive  
77 equation model which can be run in global or hemispheric modes, and is based on the  
78 spectral model of Hoskins and Simmons (1975). The vertical coordinate is the  $\sigma$   
79 terrain-following coordinate, where  $\sigma = \text{pressure}/\text{surface pressure}$ . Diabatic processes  
80 in IGCM1 include spectral hyperdiffusion to remove noise at small scales, linear or  
81 ‘Newtonian’ relaxation to a reference temperature state, and linear or ‘Rayleigh’  
82 friction at any number of model layers. Examples of research conducted with this  
83 configuration are studies of baroclinic lifecycles on Earth (Hoskins and Simmons  
84 1975, James and Gray 1986, Thorncroft et al. 1993) and Mars (Collins and James  
85 1995), as well as studies of the stationary circulation on Earth (Valdes and Hoskins  
86 1991), Mars (Joshi et al. 1994) and other planets (Joshi et al 1997).



87 In IGCM2, the linear diabatic processes in IGCM1 are replaced by more realistic  
88 nonlinear diffusive processes. Radiative processes are parameterised simply using a  
89 prescribed surface temperature and a constant cooling rate of  $1.25 \text{ Kday}^{-1}$  representing  
90 infra-red radiation to space. The effects of moisture are included in IGCM2,  
91 necessitating the inclusion of evaporation, parameterisation of deep and shallow  
92 convection, and the potential for moisture transport. Such a configuration represents  
93 moist processes allowing the study of tropical regions, and has accordingly been used  
94 in studies of mesoscale tropical dynamics and circulation (Cornforth et al. 2009).

95 IGCM3 is a full climate model in which the prescribed surface can be replaced by one  
96 or both of a two-level interactive land surface, and a slab or ‘q-flux’ ocean model. The  
97 constant radiative cooling is replaced by a radiative scheme which calculates clear sky  
98 fluxes in 2 visible bands and 6 infra-red bands, and accounts for the radiative effects  
99 of clouds. This model is described fully in an appendix to Forster et al. (2000). This  
100 configuration has been used in many studies of tropospheric climate (Forster et al  
101 | 2000, Joshi et al. 2003) and stratospheric climate (Rosier and Shine 2000, [Winter and](#)  
102 | [Bourqui 2011 a,b](#)). A coupled ocean-atmosphere model (FORTE) has been created in  
103 | the past by coupling the IGCM3 to the MOMA ocean model (e.g. Sinha et al. 2012).  
104 A similar process is underway for IGCM4, and the resulting coupled model is the  
105 subject of an accompanying paper.

106 | [We now set out the climatology of the new IGCM4 model in addition to changes](#)  
107 | [since the last published detailed version IGCM3. Section 2 details changes since](#)  
108 | [IGCM3, section 3 details the new model climatology, and section 4 details the](#)  
109 | [climatic performance of the IGCM4.](#)

110

## 111 2. Model changes from IGCM3

### 112 2.1 IGCM4 Configurations

113 IGCM4 exists in two standard configurations: a spectral truncation of T42 (having a  
114 128 x 64 horizontal grid) and 20 layers in the vertical, denoted T42L20, which is the  
115 standard configuration for studies of the troposphere and climate, and T42L35, which  
116 enables study of the stratosphere on climate. In addition, a configuration of T170L20,  
117 which enables study of mesoscale phenomena such as weather fronts and tropical  
118 waves, is also under development, but its description is beyond the scope of this paper.

119 The L20 and L35 configurations reach from the surface to 50 hPa and 0.1 hPa  
120 respectively, and are shown in Figure 1. The lowest 19 model layers in each  
121 configuration have exactly the same values, so that only the stratosphere is different,  
122 enabling more traceability when comparing different model configurations.

123 The spectral code is parallelised using a so-called 2D decomposition (Foster and  
124 Worley 1997, Kanamitsu et al. 2005). In a 2D decomposition, two of the three  
125 dimensions are divided across the processors, and so there is a column and row of  
126 processors, with the columns divided across one dimension and the rows across  
127 another. Compared with a 1D decomposition, a 2D decomposition increases the  
128 number of transpositions that need to be made to go from spectral-space to grid-space  
129 and back again. However the advantage is that each transposition is only amongst  
130 processor elements (henceforth PEs) either on the same column or the same row. Any  
131 transposition for 1D decomposition requires all the PEs to communicate with one  
132 another, which increases the size of buffers passed between PEs, communication  
133 latency, and slows down the model. Han and Juang (2004) found that a 2D  
134 decomposition is about twice as fast as a 1D decomposition. More details on the  
135 decomposition are given on the IGCM website (Stringer 2012)

136 The model's performance on a parallel cluster using an intel compiler and MPI  
137 parallelisation libraries is as follows: T42L35: ~ 75 model years/day on 32 processors;  
138 96 timesteps per day); T42L20: ~ 200 model years/day on 32 processors; 72 timesteps  
139 per day).

140

## 141 **2.2 Surface and boundary layer processes**

142 Over land, each grid point has a land-surface type based on present-day observations:  
143 there are 8 types (ice, inland water, forest, grassland, agriculture, tundra, swamp,  
144 desert). Each land-surface type has its own value for snow-free albedo A, snow-  
145 covered albedo S, the height (in metres) at which total albedo reaches  $(A+S)/2$ , and  
146 roughness length. The values of these quantities for each surface type are shown in  
147 Table 1.

148 Whenever snowmelt occurs in the model, the snowmelt moistens soil so that the soil  
149 water is 2/3 of the saturated value. This is a very simple parameterisation of snowmelt  
150 percolating through soil and helps to alleviate warm biases in late spring and summer  
151 in Eastern Eurasia, consistent with more complex GCMs such as HadGEM2 (Martin  
152 et al 2010).

153 A maximum effective depth for snow of 15m exists to prevent slow drifts in heat  
154 capacity and hence temperature and energy balance, since there is no physics in the  
155 IGCM4 to represent the melting of ice fields at their bases. In addition, the 'land ice'  
156 surface type has a fixed snow depth, so that points diagnosed as 'ice' are not subject to  
157 slowly emerging model biases in temperature appearing because of snow depth slowly  
158 being eroding away over decades. At present, these fixed land-ice points are set to be  
159 Antarctica and Greenland.

160 The effect of sea-ice in IGCM is implemented by assuming a linear change from 0°C  
161 to -2°C in these surface properties: roughness, albedo and heat capacity. This replaces  
162 the sudden change of surface properties at -2°C, which is unrealistic given partial ice  
163 cover in most oceans, and also removes a bias in that while sea-ice forms from saline  
164 water at -2°C, it melts at 0°C, since ice is mostly composed of fresh water. A  
165 combination of ice and open water is therefore desirable between -2°C and 0°C.

166 The amount that surface heat fluxes can be amplified by convectively unstable  
167 conditions above their values at neutral or zero stability has been limited to 4.0. This  
168 value has been chosen to limit latent heat fluxes over the ocean and sensible heat  
169 fluxes over the land to better match observations, although it is still a simplification of  
170 more complex schemes that involve the Richardson number (e.g. Louis 1979), since it  
171 is entirely stability-based.

172

### 173 **2.3 Radiation, convection, clouds and aerosol**

174 The NIKOSRAD radiation scheme in IGCM3 (Forster et al. 2000) has been replaced  
175 with a modified version of the Morcrette radiation scheme (Zhong and Haigh 1995)  
176 which was originally written for the ECMWF model. This is because the NIKOSRAD  
177 scheme was found to produce 2Δz oscillations under certain conditions in the  
178 stratosphere. A transitional version of IGCM3, called IGCM3.1, has existed with the  
179 Morcrette radiation scheme for some time, and many climatic (e.g. Bell et al. 2009,  
180 Cnossen et al. 2011) and climate-chemistry (e.g. Highwood and Stevenson 2003,  
181 Taylor and Bourqui 2005) studies have been conducted with it. The Morcrette  
182 radiation scheme has a representation of O<sub>3</sub> absorption of UV between 0.12μm and

183 0.25 $\mu$ m, 2 visible bands (0.25-0.68 $\mu$ m, 0.68-4 $\mu$ m), and 5 infra-red (henceforth IR)  
184 bands.

185 The radiatively active species in the IGCM are H<sub>2</sub>O, CO<sub>2</sub>, CH<sub>4</sub>, O<sub>3</sub>, N<sub>2</sub>O, CFC-11 and  
186 CFC-12. H<sub>2</sub>O is advected self-consistently in the model, but prescribed above a  
187 seasonally varying climatological tropopause. O<sub>3</sub> is specified from a zonally averaged  
188 climatology (Li and Shine 1995), which is then interpolated to model levels. All other  
189 gases are assumed to be well-mixed throughout the GCM domain, and are easily  
190 changed via a namelist.

191 The solar constant in IGCM4 is 1365 Wm<sup>-2</sup>, which is more consistent with  
192 observations than the older value of 1376 Wm<sup>-2</sup> in IGCM3 and IGCM3.1. The ocean  
193 albedo A<sub>o</sub> varies with latitude  $\varphi$  in this manner:

$$194 \quad A_o = 0.45 - 0.30\cos \varphi. \quad (1)$$

195 This is a simple parameterisation of the effects of aerosols and solar zenith angle on  
196 albedo based on observations so that at the equator A<sub>o</sub> = 0.15, increasing to 0.3 at  
197 60°S/N.

198 The convection scheme in the IGCM4 is identical to that described in Forster et al  
199 (2000) and is based on the scheme of Betts (1986), with separate adjustment processes  
200 for shallow and deep convection; the adjustment process for deep convection takes  
201 place over 3 hours as in Forster et al (2000). Rainout of shallow convective  
202 precipitation is now allowed in IGCM4 over a timescale of 6 hours. This rainout helps  
203 to slow down the Hadley circulation, whilst removing some of the shallow convective  
204 cloud that occurs over subtropical regions. Stratiform precipitation is as in Forster et  
205 al (2000): grid-scale supersaturation is removed. Above a gridpoint relative humidity

206 | (henceforth RH) of 0.8, clouds are formed whose fraction F is given by  $F = ((RH -$   
207 |  $0.8)/0.2)^2$ . No cloud can form in the very lowest model layer.

208 | The clouds have been tuned to better match observations of outgoing infra-red  
209 | radiation and downward surface solar radiation: the cloud base fraction for deep  
210 | convective cloud is 4 times the fraction at all other levels, which is consistent with  
211 | observed convective cloud profiles (Slingo 1987). A version of the Kawai and Inoue  
212 | (2006) parameterisation for marine stratocumulus cloud has also been implemented in  
213 | IGCM4. This diagnoses low cloud at ocean points depending on the stability of the  
214 | lowest two model sigma half layers, i.e. between the surface and layer 1, and layer 1  
215 | and layer 2, and deposits cloud in the second-to-lowest model layer if diagnosed.

216 | Aerosols are not in the standard IGCM4: their effect on surface temperatures have  
217 | been parameterised by slightly raising the albedo of land and ocean by 0.05. This is  
218 | because even CMIP5 GCMs have trouble accurately representing the forcing due to  
219 | different types of aerosol. In addition, even the aerosol scheme in the IGCM only  
220 | deals with the direct effect, and not the different indirect effects such as cloud lifetime  
221 | and particle size that are also present in reality. However, both specific case studies of  
222 | tropospheric and stratospheric aerosols have been studied using IGCM3.1 (Highwood  
223 | and Stevenson 2003, Ferraro et al. 2014), so future study using IGCM4 remains  
224 | technically very feasible.

225

## 226 | **2.4 Stratosphere**

227 | A simple gravity wave drag scheme based on Lindzen (1981) had previously been  
228 | implemented in both IGCM1 (Joshi et al 1995) and IGCM3 (Cnossen et al. 2011).

229 | The IGCM4 scheme is as above, but calculates drag based on orographic drag, as well

230 as 2 non-orographic modes having horizontal phase speeds of  $\pm 10 \text{ ms}^{-1}$ . The  
231 orographic drag source amplitude is the magnitude of the zonal wind in the lowest  
232 model layer multiplied by the subgrid-scale standard deviation of topography; the  
233 non-orographic source amplitude is the magnitude of the zonal wind in the lowest  
234 model layer multiplied by a constant value of 90m.

235 | Stratospheric water vapour (henceforth SWV) is calculated by adding a fixed value (3  
236 | ppmv) onto an amount calculated by a parameterisation that considers the  
237 | stratospheric radiative effects of changing tropospheric methane concentrations.  
238 Methane oxidation in the stratosphere depends on the stratospheric chemical  
239 environment and stratospheric residence time. While both the chemical environment  
240 and the Brewer-Dobson circulation may change in a changing climate, coupled  
241 chemistry-climate model integrations show that their effects on stratospheric methane  
242 (and hence on SWV) is small compared to the effect of the changes in methane  
243 entering the stratosphere (Eyring et al 2010), which in turn is given by the change in  
244 average tropospheric methane to a good approximation. Hence, the impact of  
245 changing tropospheric methane can be approximated by calculating the stratospheric  
246 distribution of the fraction of oxidised methane, which then is multiplied by the  
247 amount of tropospheric methane to give the change in stratospheric methane and its  
248 contribution to changes in SWV. We define the oxidised fraction  $\beta$ :

$$249 \quad \beta(\varphi, z) = 1 - CH_4(\varphi, z) / CH_4_{troposphere} \quad (2)$$

250 | where  $z$  is altitude,  $\varphi$  is latitude, and any longitudinal variation is assumed to be  
251 | averaged.  $CH_4(\varphi, z)$  is obtained from satellite measurements by the Halogen  
252 | Occultation Experiment (HALOE, Russell et al. 1993) over the period 1995-2005.  
253 Assuming that two water molecules form for each methane molecule, the water  
254 vapour change occurring over a given time interval is given by combining the change

255 in CH<sub>4</sub> over the same time interval with the scaling factor  $\beta$  in a similar manner to  
256 Fueglistaler and Haynes (2005) giving:

$$257 \quad dH_2O(\varphi, z) = 2 * \beta(\varphi, z) * dCH_{4troposphere} \quad (3)$$

258 These calculated SWV anomalies are then supplied to the IGCM to allow calculation  
259 of the influence of this additional effect on climate. This approach provides excellent  
260 predictions of stratospheric methane changes in CCMVal2 models for the period  
261 1960-2008 (REF-1B runs) [\(Eyring et al 2010\)](#).

262 Figure 2 (top right) shows an analytical approximation to this distribution, which is  
263 then used to calculate  $\beta$ . The effect is demonstrated by showing the SWV perturbation  
264 in ppmv for pre-industrial CH<sub>4</sub> concentrations of 0.75 ppmv (bottom left), and  
265 potential future concentrations of CH<sub>4</sub> of 2.5 ppmv (bottom right), [as might be](#)  
266 [expected in the mid 21<sup>st</sup> century under the Representative Concentration Pathway](#)  
267 [\(RCP\) 8.5 scenario \(Holmes et al 2013\)](#). For reference the background SWV  
268 concentration to which this perturbation is added is 3 ppmv.

269

### 270 **3. Model Evaluation**

#### 271 **3.1 Surface and top-of-atmosphere model climatology**

272 The following results are all from the most commonly used configuration of the  
273 IGCM4: sea surface temperature (henceforth SST) is prescribed [as](#) a monthly-varying  
274 climatology [based on ERA-40 reanalysis](#) (Forster et al 2000), but land temperature is  
275 calculated self-consistently from surface fluxes at each timestep. For this section, the  
276 20-layer T42L20 model has been used, which has been integrated for [100](#) model years  
277 in total.



278 Figure 3 shows the comparison between NCEP-DOE Reanalysis 2 (Kanamitsu et al.  
279 2002) and IGCM4 surface temperature. During Boreal winter (December- February,  
280 or DJF), Figure 3 (bottom left panel) shows that the model displays a slight cold bias  
281 in Northern Eurasia, and a warm bias in the tropical regions and Antarctica. The bias  
282 is mostly below 10K in amplitude, which is good for intermediate models of this type.  
283 The boreal summer response (June-August, or JJA) is shown in Figure 3 (bottom right  
284 panel). Here, a warm bias is present over most of the land surface. The warm bias in  
285 both summer hemispheres is likely due to an absence of aerosols in the IGCM,  
286 especially over North Africa and Australia where high amounts of dust occur in  
287 reality. However, even during JJA the magnitude of the bias is less than 10K almost  
288 everywhere, which is reasonable when compared to biases even in CMIP5 models  
289 (e.g. Flato et al. 2013, Figure 9.2). Both ice caps display too large a seasonal cycle,  
290 which we attribute to the simplicity of the snow scheme in the model, which has no  
291 facility for changing density or conductivity when snow is compacted into ice. This  
292 could be a source for future model improvement.

293 Figure 4c (top right panel) shows the precipitation bias in DJF in the IGCM compared  
294 to the CMAP dataset (Xie and Arkin 1997) shown in Figure 4a (top left panel). In  
295 general the comparison is quite good, with the major convergence zones (as diagnosed  
296 by the 4 mm day<sup>-1</sup> contour in black) being represented quite well. As a guide to the  
297 IGCM's performance in the context of other models, the mean  $\pm$  one standard  
298 deviation precipitation bias amongst a subset of models present in the CMIP5 archive  
299 being used for the UN Intergovernmental Panel on Climate Change's 5<sup>th</sup> assessment  
300 report (IPCC AR5) is also shown (Figures 4d and 4f respectively): the comparison is  
301 for the CMIP5 model configuration using prescribed "AMIP" SSTs, since coupled  
302 ocean-atmosphere biases tend to worsen model performance.

303 | The IGCM's precipitation bias (top right panel) lies within one standard deviation of  
304 | the AMIP ensemble biases; for instance the dry bias in the Southern Pacific  
305 | Convergence Zone (SPCZ) in the IGCM (top left panel) is 2-5 mm day<sup>-1</sup>, which is  
306 | similar in magnitude to the mean minus one standard deviation, suggesting that the  
307 | IGCM's performance in this region is within the envelope of state-of-the-art GCMs  
308 | forced by observed SSTs.

309 | Figure 5 is the same as Figure 4, but for the JJA period. There are some notable wet  
310 | biases in IGCM4 as shown by Figure 5c (top right panel), particularly in the northern  
311 | Indian Ocean and Central American regions: however such wet biases are not outside  
312 | the envelope of the CMIP5 ensemble when comparing the IGCM to the "mean plus  
313 | one standard deviation" (Figure 5f- bottom right panel). Thus, for the JJA season as  
314 | well as the DJF season, the precipitation bias in IGCM4 is within the range of state-  
315 | of-the-art GCMs forced by observed SSTs, which provides a good justification for the  
316 | use of IGCM4 as a simplified climate model.

317 | The interaction of precipitation, cloud and radiation, can be studied by comparing the  
318 | outgoing long-wave radiation (OLR) field with observations (Liebmann and Smith  
319 | 1996), which is shown in Figure 6. The bottom left panel shows that the IGCM  
320 | broadly simulates OLR quite well, with some differences between model and  
321 | observations in the Maritime continent region. During JJA (bottom right panel), there  
322 | is a positive bias in OLR over the Indian Ocean (Figure 6f- bottom right panel),  
323 | consistent with a slight dry bias there (Figure 4c). The top-of-atmosphere energy  
324 | imbalance in the IGCM is approximately 1-2 Wm<sup>-2</sup>, which is similar to other climate  
325 | models (e.g. Roeckner et al. 2006).

326

## 327 3.2 Zonal mean climatology and stratospheric performance

328 For this section, both 20-layer T42L20 and 35-layer T42L35 configurations are  
329 described; the latter has been integrated for 200 model years in total, in order to  
330 average out the effect of stratospheric variability. Figure 7 shows the zonally averaged  
331 temperature structure in IGCM4 for the two solstitial seasons compared to data from  
332 the ERA40 reanalysis (Uppala et al 2005). In both seasons the lower stratosphere in  
333 both L20 and L35 configurations is too cold in the tropics and the winter extratropics  
334 by 5-10K. Elsewhere, biases are smaller than 10 K apart from near the summer  
335 stratopause, perhaps due to deficiencies in the ozone heating in IGCM4. These errors  
336 are comparable models that represent the stratosphere (e.g. Eyring et al. 2006).

337 A comparison between the zonally-averaged zonal wind in IGCM4 and ERA40 is  
338 shown in Figure 8, and like Figure 7, also shows good agreement, perhaps not  
339 surprisingly for a field that is expected to be in large-scale thermal balance with  
340 temperature. In both L20 and L35 configurations, the southern hemisphere  
341 tropospheric jetstream is slightly equatorward of the jet in ERA40 as shown by the  
342 dipole pattern in colours in Figures 8 c-f in this region. During DJF the northern  
343 hemisphere's tropospheric jetstream is slightly too strong in both L20 (Figure 8c) and  
344 L35 (Figure 8e) by 5 ms<sup>-1</sup>. In general, both L20 and L35 configurations display  
345 similar tropospheric biases in zonal wind.

346 During DJF, the strength of the stratospheric jetstreams in the L35 configuration  
347 IGCM4 compares well to ERA40 (Figure 7e). In northern winter especially this is a  
348 sign that the joint effects of gravity wave drag and tropospheric wave forcing in  
349 IGCM4 are approximately of the right magnitude, since these two factors play a  
350 crucial role in controlling the strength of the DJF winter stratospheric jetstream. In  
351 JJA however the stratospheric jetstream is weaker and less tilted in the vertical than

352 | ERA40 (Figure 7f). This bias is likely due to the simplicity of the gravity wave drag  
353 | scheme (see above), and might be removed by more tuning of the drag scheme- but  
354 | this would require more multi-century L35 integrations to ensure that tuning did not  
355 | result in greater biases elsewhere; as such it is a source for future development.

356 | The zonally asymmetric component of the circulation is apparent from Figure 9,  
357 | which shows the geopotential height eddy fields at 500 and 200 hPa. The IGCM4  
358 | reproduces the main features of the reanalysis with the standing wave patterns  
359 | apparent in both model configurations, although low pressure anomaly in NE Asia is  
360 | weaker in both model configurations compared to reanalysis. Both L35 and L20  
361 | configurations display a similar standing wave pattern at both pressure levels.

362 | A key issue for stratospheric dynamics and its interplay with tropospheric climate,  
363 | which is a primary use of this model, is that the stratospheric circulation, and  
364 | phenomena such as sudden stratospheric warmings (henceforth SSWs) are simulated  
365 | as well as other models. A 200-year long integration of IGCM4 yielded 0.57 SSWs  
366 | per year as diagnosed by the method of Charlton and Polvani (2007); this should be  
367 | compared with 0.6 as diagnosed in reanalyses by Charlton and Polvani (2007). 57% of  
368 | the SSWs were categorised as “displacement” events using a vortex moment method  
369 | based on Mitchell et al. (2011), and 43% diagnosed as “split” events, again broadly  
370 | consistent with reanalysis output which suggests that just under half of SSWs can be  
371 | categorised as “split” events (Charlton and Polvani 2007). The timing of SSWs  
372 | during boreal winter is shown in Figure 10. Again, the timings are broadly consistent  
373 | with reanalysis output, although there are somewhat more displacement events during  
374 | March than diagnosed from reanalysis.

375

#### 376 | **4. Climate Change and Energy Balance**

377 | When coupled to a slab q-flux ocean model, IGCM4 has an equilibrium climate  
378 | sensitivity when doubling CO<sub>2</sub> from its pre-industrial concentration of 280 ppmv of  
379 | 2.1K. This sensitivity is slightly higher than the value of 1.6K in IGCM3 (Joshi et al  
380 | 2003), and is likely due to the changes in cloud physics outlined above.

381 | We have not performed simulations of a slab model for this paper because although  
382 | one effect of a slab ocean is to change the characteristics of model interannual  
383 | variability (as shown by Winter and Bourqui 2011a), the nature of such changes will  
384 | depend on the depth of the slab, and how this depth changes seasonally and  
385 | geographically: for instance in the North Atlantic Ocean the effective mixed layer  
386 | depth changes from 50 m during summer to 500 m in winter. Moreover, the dynamic  
387 | influence of the atmosphere on the ocean will also depend on the effective mixed  
388 | layer depth of the ocean, or depth of the slab, as shown by O' Callaghan et al (2014),  
389 | as well as causing a dynamical ocean response (Zhai et al 2014).

390 | Because interannual variability is sensitive to slab ocean depth, and the IGCM has a  
391 | constant slab depth, rather than one that varies seasonally and geographically, we  
392 | have not discussed interannual variability in this paper. However, such a topic would  
393 | be a source of useful research in the future for a configuration of the IGCM that had  
394 | such a varying slab ocean model.

395 | As a first assessment of coupled model performance, the zonally averaged net surface  
396 | energy imbalance and wind stress curl in IGCM4 are examined and compared to  
397 | reanalysis, since large errors in these two fields will give errors in the dynamic and  
398 | thermodynamic ocean responses respectively. Figure 11 shows that the broad patterns  
399 | of response are similar in both model and reanalysis. In equatorial regions incoming

400 solar radiation is not quite balanced by outgoing IR emission because of the presence  
401 of tropical convection and thick clouds, leading to positive values (see top panel); the  
402 intense rainfall associated with such convection is shown in the top panels of Figures  
403 4 and 5. In subtropical regions, a lack of cloud leads to more IR emission and negative  
404 values in both reanalysis and IGCM4. The pattern of wind stress curl (see bottom  
405 panel) is indicative of the combined effects of midlatitude westerlies, and subtropical  
406 and tropical trade winds, and is similar in both model and reanalysis apart from the  
407 southern ocean westerlies being slightly too equatorward in the model, and the Arctic,  
408 where the IGCM fails to reproduce large values associated with mesoscale  
409 circulations (e.g. Condrón and Renfrew 2013) that the model cannot represent given  
410 its horizontal resolution.

411 To summarise, we have presented the physical details, and major climatological and  
412 dynamical features of the IGCM4 climate model. The model provides a fast  
413 alternative to conventional state-of-the-art GCMs while retaining the richness of  
414 dynamical behaviour allowed by the primitive equations of meteorology. As such the  
415 IGCM4 forms a useful part of the “hierarchy of models” approach needed to fully  
416 understand climate.

417

## 418 **5. Acknowledgements**

419 Model simulations were carried out on the High Performance Computing Cluster  
420 supported by the Research and Specialist Computing Support service at the University  
421 of East Anglia. AOC acknowledges the support of the UK Natural Environment  
422 Research Council (NERC). OLR and CMAP Precipitation data provided by the  
423 NOAA/OAR/ESRL PSD, Boulder, Colorado, USA, from their Web site at

424 <http://www.esrl.noaa.gov/psd/>. We acknowledge the assistance of M. Blackburn, D.  
425 Stevens, B. Sinha, A. Blaker, A. Ferraro, E. Highwood, K. Shine and C. Bell.

426

427

## 428 **6. Code Availability**

429 The code is available to scientific researchers on request by emailing  
430 [m.joshi@uea.ac.uk](mailto:m.joshi@uea.ac.uk) in the first instance. Websites detailing different IGCM  
431 configurations are given in section 2.2. IGCM4 requires as a prerequisite a fortran  
432 compiler, the nupdate code management utility, and MPI routines for parallel  
433 integrations (although IGCM4 is designed to run on one processor).

434

## 435 **7. References**

436 Bell, C., Gray, L. J., Charlton-Perez, A., Joshi, M. M., and Scaife, A.: Stratospheric  
437 Communication of El Niño Teleconnections to European Winter, *J. Climate*, 22,  
438 4083-4096, 2009.

439 Charlton, A. J., and Polvani, L. M.: A new look at stratospheric sudden warmings.  
440 Part I: Climatology and modeling benchmarks, *J. Climate*, 20, 449-469, 2007.

441 Cnossen, I., Lu, H., Bell, C. J., Gray, L. J., and Joshi, M. M.: Solar signal propagation:  
442 The role of gravity waves and stratospheric sudden warmings, *J. Geophys. Res.*, 116,  
443 DOI: 10.1029/2010JD014535, 2011.

444 Collins, M., and James, I. N.: Regular baroclinic transient waves in a simplified global  
445 circulation model of the Martian atmosphere, *J. Geophys. Res.*, 100, 14421–14432,  
446 1995.

447 Condrón, A. and Renfrew, I. A.: The impact of polar mesoscale storms on northeast  
448 Atlantic Ocean circulation, *Nat. Geos.*, 6, 34–37, 2013.

449 [Cornforth, R. J., Hoskins, B. J., and Thorncroft, C. D.: The impact of moist process on](#)  
450 [the African easterly jet- African easterly wave system, \*Q. J. R. Meteorol. Soc.\*, 135,](#)  
451 [894-913, 2009.](#)

452 Eyring, V., et al.: Assessment of temperature, trace species, and ozone in chemistry-  
453 climate model simulations of the recent past, *J. Geophys. Res.*, 111, D22308,  
454 DOI:10.1029/2006JD007327, 2006.

455 Eyring, V., Shepherd, T.G., and Waugh, D. W. (Eds.): [SPARC Report on the](#)  
456 [Evaluation of Chemistry-Climate Models](#), SPARC Report No. 5, WCRP-132,  
457 WMO/TD-No. 1526, 2010.

458 Ferraro, A. J., Highwood, E. J., and Charlton-Perez, A. J., Weakened tropical  
459 circulation and reduced precipitation in response to geoengineering, *Environ. Res.*  
460 *Lett.*, DOI:10.1088/1748-9326/9/1/014001, 2014.

461 Flato, G., Marotzke, J., Abiodun, B., Braconnot, P., Chou, S. C., Collins, W., Cox, P.,  
462 Driouech, F., Emori, S., Eyring, V., Forest, C., Gleckler, P., Guilyardi, E., Jakob, C.,  
463 Kattsov, V., Reason, C., and Rummukainen, M. : Evaluation of Climate Models. In:  
464 *Climate Change 2013: The Physical Science Basis. Contribution of Working Group I*  
465 *to the Fifth Assessment Report of the Intergovernmental Panel on Climate Change*  
466 [Stocker, T.F., D. Qin, G.-K. Plattner, M. Tignor, S.K. Allen, J. Boschung, A. Nauels,  
467 Y. Xia, V. Bex and P.M. Midgley (eds.)]. Cambridge University Press, Cambridge,  
468 United Kingdom and New York, NY, USA, 2013.



469 Foster, I. T., and Worley, P. H.: Parallel Algorithms For The Spectral Transform  
470 Method, SIAM Journal on Scientific Computing, 18, 806–837.  
471 DOI:10.2172/10168301, 1997.

472 Forster, P. M. De F., Blackburn, M., Glover, R., and Shine, K. P.: An examination of  
473 climate sensitivity for idealised climate change experiments in an intermediate general  
474 circulation model. Climate Dynamics, 16, 833-849, 2000.

475 Fueglistaler, S., and Haynes, P.H.: Control of interannual and longer-term variability  
476 of stratospheric water vapor, J. Geophys. Res., 110, DOI:10.1029/2005JD006019,  
477 2005.

478 Han, J., and Juang, H.-M.: Development of Fully Parallelized Regional Spectral  
479 Model at NCEP. 20<sup>th</sup> Conference on Weather Analysis and Forecasting, Seattle, Amer.  
480 Meteor. Soc., 2004. Available at <https://ams.confex.com/ams/pdfpapers/71807.pdf>

481 Highwood, E. J., and Stevenson, D.: Atmospheric impact of the 1783-1784 Laki  
482 eruption: Part 2 Climate effect of sulphate aerosol. Atm. Chem. Phys., 3, 1177-1189,  
483 2003.

484 [Holmes, C. D., Prather, M. J., Søvde, O. A. and Myhre, G: Future methane, hydroxyl,](#)  
485 [and their uncertainties: key climate and emission parameters for future predictions,](#)  
486 [Atmos. Chem. Phys., 13, 285-302, 2013.](#)

487 Hoskins, B. J., and Simmons, A. J: A multilayer spectral model and the semi-implicit  
488 method, Q. J. R. Meteorol. Soc., 101, 637-655, 1975.

489 James, I. N., and Gray, L. J.: Concerning the effect of surface drag on the circulation  
490 of a baroclinic planetary atmosphere, Q. J. R. Meteorol. Soc., 114, 619-637, 1986.

491 Joshi, M. M., Lewis, S. R., Read, P. L., and Catling, D. C.: Western boundary currents  
492 in the atmosphere of Mars, Nature, 367, 548-552, 1994.

493 Joshi, M. M., Lawrence, B. N., and Lewis, S. R.: Gravity wave drag in three-  
494 dimensional atmospheric models of Mars, *J. Geophys. Res.*, 100, 21235-21245, 1995.

495 Joshi, M. M., Haberle, R. M., and Reynolds, R. T.: Simulations of the atmospheres of  
496 synchronously rotating terrestrial planets orbiting M-dwarfs: conditions for  
497 atmospheric collapse and implications for habitability, *Icarus*, 29, 450-465, 1997.

498 Joshi, M. M., Shine, K. P., Ponater, M., Stuber, N., Sausen, R., and Li, L.: A  
499 comparison of climate response to different radiative forcings in three general  
500 circulation models: Towards an improved metric of climate change, *Climate*  
501 *Dynamics*, 20, 843-854, 2003.

502 Kanamitsu, M., Ebisuzaki, W., Woollen, J., Yang, S-K., Hnilo, J. J., Fiorino, M., and  
503 Potter, G L.: NCEP-DOE AMIP-II Reanalysis (R-2), *Bull. Amer. Meteorol. Soc.*,  
504 1631-1643, 2002.

505 Kanamitsu, M., Kanamaru, H., Cui, Y., and H. Juang: Parallel Implementation of the  
506 Regional Spectral Atmospheric Model. Scripps Institution of Oceanography,  
507 University of California at San Diego, and National Oceanic and Atmospheric  
508 Administration for the California Energy Commission, PIER Energy-Related  
509 Environmental Research. CEC-500-2005-014, 2005.

510 Kawai, H., and Inoue, T.: A simple parameterisation scheme for subtropical marine  
511 stratocumulus, *SOLA*, 2, 017-020, DOI:10.2151/sola.2006-005, 2006.

512 Li, D. and K. P. Shine, A 4-Dimensional Ozone Climatology for UGAMP Models,  
513 UGAMP Internal Report No. 35, April 1995.

514 Liebmann, B. and Smith, C. A.: Description of a complete (interpolated) outgoing  
515 longwave radiation dataset, *Bull. Amer. Meteorol. Soc.*, 77, 1275-1277, 1996.

516 Lindzen, R. S: Turbulence and stress owing to gravity wave and tidal breakdown, J.  
517 Geophys. Res., 86, 9707-9714, 1981.

518 Louis, J. F.: A parametric model of vertical eddy fluxes in the atmosphere, Bound.-  
519 Layer Meteor., 17, 187–202, 1979.

520 Martin, G. M., Milton, S. F., Senior, C.A., Brooks, M. E., Ineson, S., Reichler, T. and  
521 Kim, J.: Analysis and Reduction of Systematic Errors through a Seamless Approach  
522 to Modeling Weather and Climate, J. Climate, 23, 5933–5957, 2010.

523 Mitchell, D. M., Charlton-Perez, A. J., and Gray, L.J.: Characterising the Variability  
524 and Extremes of the Stratospheric Polar Vortices Using 2D Moments, J. Atmos. Sci.,  
525 1194-1213, 2011.

526 O' Callaghan, A., Joshi M. M., Stevens, D. P. and Mitchell: The effects of different  
527 sudden stratospheric warming types on the ocean, Geophys. Res. Lett. 41, 7739–7745,  
528 2014, DOI: 10.1002/2014GL062179, 2014.

529 Roeckner , E., Brokopf , R., Esch , M., Giorgetta , M., Hagemann, S. Kornblueh, L.,  
530 Manzini, E., Schlese U., and Schulzweida, U.: Sensitivity of Simulated Climate to  
531 Horizontal and Vertical Resolution in the ECHAM5 Atmosphere Model, J. Climate,  
532 19, 3771–3791, 2006.

533 Rosier, S. M., and Shine, K. P.: The effect of two decades of ozone change on  
534 stratospheric temperature as indicated by a general circulation model, Geophys. Res.  
535 Lett., 27, 2617-2620, 2000.

536 Russell, J. M. III, Gordley. L. L., Park, J. H., Drayson, S. R., Hesketh, W. D.,  
537 Cicerone, R. J., Tuck, A. F., Frederick, J. E., Harries, J. E., Crutzen, P. J.: The  
538 Halogen Occultation Experiment, J. Geophys. Res., 98, 10777 – 10798, 1993.

539 | [Sinha, B., Hirschi, J., Bonham, S., Brand, M., Josey, S. A., Smith, R. and Marotzke,](#)  
540 | [J.: Mountain ranges favour vigorous Atlantic Thermohaline Circulation, Geophys.](#)  
541 | [Res. Lett., 39, L02705, DOI:10.1029/2011GL050485, 2012.](#)

542 | Slingo, J. M.: The development and verification of a cloud prediction scheme for the  
543 | ECMWF model, Q. J. R. Meteorol. Soc., 113, 899-927, 1987.

544 | [Stringer M.: http://www.met.reading.ac.uk/~lem/large\\_models/igcm/parallel/, 2012](#)

545 | [Taylor, C. P., and Bourqui, M. B.: A new fast stratospheric ozone chemistry scheme](#)  
546 | [in an intermediate general-circulation model. I: Description and evaluation, Quart. J.](#)  
547 | [Royal. Meteorol. Soc., 131, 2225-2242, 2005.](#)

548 | Thorncroft, C. D., Hoskins, B. J., and McIntyre, M. E.: Two paradigms of baroclinic  
549 | lifecycle behaviour, Q. J. R. Meteorol. Soc., 119, 17-55, 1993.

550 | Uppala, S.M., Kållberg, P.W., Simmons, A.J., Andrae, U., da Costa Bechtold, V.,  
551 | Fiorino, M., Gibson, J.K., Haseler, J., Hernandez, A., Kelly, G.A., Li, X., Onogi, K.,  
552 | Saarinen, S., Sokka, N., Allan, R.P., Andersson, E., Arpe, K., Balmaseda, M.A.,  
553 | Beljaars, A.C.M., van de Berg, L., Bidlot, J., Bormann, N., Caires, S., Chevallier, F.,  
554 | Dethof, A., Dragosavac, M., Fisher, M., Fuentes, M., Hagemann, S., Hólm, E.,  
555 | Hoskins, B.J., Isaksen, L., Janssen, P.A.E.M., Jenne, R., McNally, A.P., Mahfouf, J.-  
556 | F., Morcrette, J.-J., Rayner, N.A., Saunders, R.W., Simon, P., Sterl, A., Trenberth,  
557 | K.E., Untch, A., Vasiljevic, D., Viterbo, P., and Woollen, J.: The ERA-40 re-analysis.  
558 | Quart. J. R. Meteorol. Soc., 131, 2961-3012, 2005.

559 | [Valdes, P. J., and Hoskins, B. J.: Nonlinear Orographically Forced Planetary Waves, J.](#)  
560 | [Atmos. Sci., 48, 2089–2106, 1991.](#)

561 [Winter B. and Bourqui, M. S.: The Impact of Surface Temperature Variability on the](#)  
562 [Climate Change Response in the Northern Hemisphere Polar Vortex. Geophys. Res.](#)  
563 [Lett., 38, L08808, doi:10.1029/2011GL047011, 2011a.](#)

564 [Winter B. and Bourqui, M. S.: Sensitivity of the Stratospheric Circulation to the](#)  
565 [Latitude of Thermal Surface Forcing. J. Climate, 24, 5397–5415, 2011b.](#)

566 Xie P., and Arkin, P. A.: Global precipitation: a 17-year monthly analysis based on  
567 gauge observations, satellite estimates, and numerical model outputs. Bull. Amer.  
568 Meteor. Soc., 78, 2539-2558, 1997.

569 Zhai, X., Johnson, H. L., and Marshall, D. P.: A simple model of the response of the  
570 Atlantic to the North Atlantic Oscillation, J. Climate, doi:10.1175/JCLI-D-13-00330.1,  
571 in press, 2014.

572 Zhong W.Y., and Haigh, J. D.: Improved broad-band emissivity parameterization for  
573 water vapor cooling calculations. J. Atmos. Sci., 52, 124-138, 1995.

574 **8. Table Captions**

575 Table 1: Values of surface characteristics for each surface type in IGCM4(ice, inland  
 576 water, forest, grassland, agriculture, tundra, swamp, desert).

<u>Surface Type</u>	<u>Albedo</u>	<u>Snow-covered albedo</u>	<u>Height when albedo is snow-covered (m)</u>	<u>Roughness length (m)</u>
<u>Ice</u>	<u>0.8</u>	<u>0.8</u>	<u>0.05</u>	<u>0.03</u>
<u>Inland Water</u>	<u>0.2</u>	<u>0.6</u>	<u>0.05</u>	<u>0.001</u>
<u>Forest</u>	<u>0.25</u>	<u>0.7</u>	<u>0.1</u>	<u>0.1</u>
<u>Grassland</u>	<u>0.25</u>	<u>0.8</u>	<u>0.1</u>	<u>0.05</u>
<u>Agriculture</u>	<u>0.25</u>	<u>0.8</u>	<u>0.1</u>	<u>0.05</u>
<u>Tundra</u>	<u>0.3</u>	<u>0.8</u>	<u>0.05</u>	<u>0.03</u>
<u>Swamp</u>	<u>0.2</u>	<u>0.8</u>	<u>0.05</u>	<u>0.03</u>
<u>Desert</u>	<u>0.3</u>	<u>0.8</u>	<u>0.05</u>	<u>0.03</u>

577

578

579

580

581

582

583 | **9. Figure Captions**

584 | Figure 1: Model layer index vs pressure (for a surface pressure of 1000 hPa) for the  
585 | 35 layer model (black) and the 20 layer model (red). Note that the lowest 19 layers are  
586 | exactly the same for both configurations.

587 | Figure 2: The fraction of oxidised methane (which is linked to CH<sub>4</sub> concentration- see  
588 | equation 1) derived from HALOE data (top left panel); the analytical approximation  
589 | which extends to the poles (top right panel); the perturbation to stratospheric water  
590 | vapour (SWV) (ppmv) in pre-industrial conditions, when CH<sub>4</sub> is 0.75 ppmv (bottom  
591 | left); the perturbation to SWV (ppmv) if CH<sub>4</sub> is increased to 2.5 ppmv (bottom right).

592 | Figure 3: Surface temperature (°C) in IGCM4 (a,b), NCEP-DOE reanalysis (c,d) and  
593 | difference between IGCM4 and reanalysis (e,f). In all cases the left-hand panels  
594 | display results for the DJF season and the right-hand panels display results for JJA  
595 | season. For the reanalysis a mean over the years 1979-2013 is taken.

596 | Figure 4: DJF season mean precipitation (mm day<sup>-1</sup>) in CMAP (a), IGCM4 (b) and  
597 | difference between IGCM4 and CMAP (c). Subfigure (e) shows the difference  
598 | between a multi model mean of an ensemble of CMIP5 GCMs integrated using AMIP  
599 | SSTs and CMAP; (f) as for (e) but for the multi model mean minus one standard  
600 | deviation; (g) as for (e) but for the multi model mean plus one standard deviation. In  
601 | all cases the solid line is the 4 mm day<sup>-1</sup> contour in CMAP and the dashed line is the  
602 | same contour in the model of the subfigure. Subfigures (a,b) are based on the top  
603 | colour bar, subfigures (c-f) are based on the bottom colour bar. The CMIP5 models  
604 | used in the ensemble are: ACCESS1.0, ACCESS1.3, BCC-CSM1.1, BCC-  
605 | CSM1.1(m), BNU-ESM, CanCM4, CCSM4, CESM1(CAM5), CCMC-CM, CNRM-  
606 | CM5, CSIRO-Mk3.6.0, FGOALS-g2, GFDL-CM3, GISS-E2-R, HadGEM2-AO,

607 INM-CM4, IPSL-CM5A-LR, IPSL-CM5A-MR, IPSL-CM5B-LR, MIROC5, MPI-  
608 ESM-LR, MPI-ESM-MR, MRI-CGCM3, NorESM1-M, mean over the years 1979-  
609 2005.

610 Figure 5: As for Figure 4, but during the JJA season.

611 Figure 6: Outgoing longwave radiation or OLR ( $W m^{-2}$ ) in IGCM4 (a,b), interpolated  
612 OLR dataset (c,d) and difference between IGCM4 and interpolated OLR dataset  
613 (Liebmann and Smith 1996) (e,f). In all cases the left-hand panels display results for  
614 the DJF season and the right-hand panels display results for JJA season. For the  
615 interpolated OLR dataset a mean over the years 1979-2011 is taken.

616 Figure 7: Zonally averaged temperature (K) in ERA (a,b), difference between IGCM4  
617 L20 and ERA (c,d) and difference between IGCM4 L35 and ERA (e,f) in colour  
618 shading. In all subfigures contours show the total zonal mean temperature field  
619 (contour interval is 10 K, 240K contour thicker). In all cases the left-hand panels  
620 display results for the DJF season and the right-hand panels display results for JJA  
621 season. For the reanalysis a mean over the years 1958-2002 is taken.

622 Figure 8: Zonally averaged zonal wind ( $ms^{-1}$ ) in ERA (a,b), difference between  
623 IGCM4 L20 and ERA (c,d) and difference between IGCM4 L35 and ERA (e,f) in  
624 colour shading. In all subfigures contours show the total zonal mean zonal wind field  
625 (contour interval is  $10 ms^{-1}$ , negative contours dashed, zero contour dotted). In all  
626 cases the left-hand panels display results for the DJF season and the right-hand panels  
627 display results for JJA season. For the reanalysis a mean over the years 1958-2002 is  
628 taken.



629 | Figure 9: Geopotential Height (m) DJF Eddy Fields for: (a), (b) 200 hPa and 500 hPa  
630 | ERA-40 Reanalysis respectively. The same for (c), (d) IGCM4 L20 and (e), (f)  
631 | IGCM4 L35. For the reanalysis a mean over the years 1958-2002 is taken.

632 | Figure 10: Distribution of sudden stratospheric warmings in boreal winter by month in  
633 | the IGCM4 (filled grey boxes) and reanalysis (red outline boxes) (top panel);  
634 | distribution of displacement-type warmings (middle panel); distribution of split-type  
635 | warmings (bottom panel).

636 | Figure 11: Annually averaged net downward zonal surface energy imbalance ( $\text{Wm}^{-2}$ )  
637 | in IGCM4 (black) and NCEP reanalysis (red) (top panel); Wind stress curl ( $10^{-7}\text{Nm}^{-3}$ )  
638 | in IGCM4 (black) and NCEP reanalysis (red) (bottom panel).

639

640

641

642

643

644

645

646

647

648

649

650

651

652

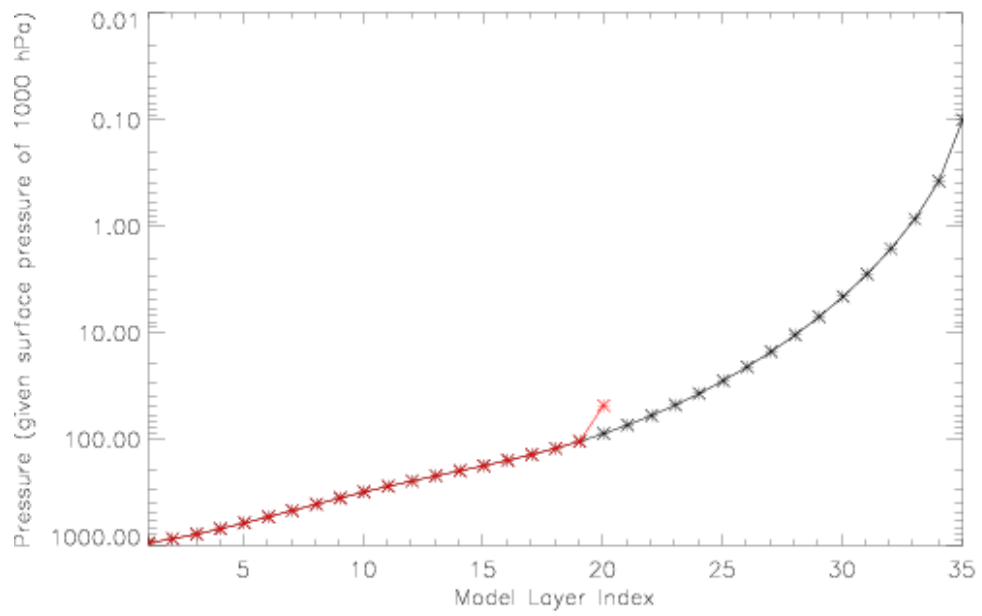
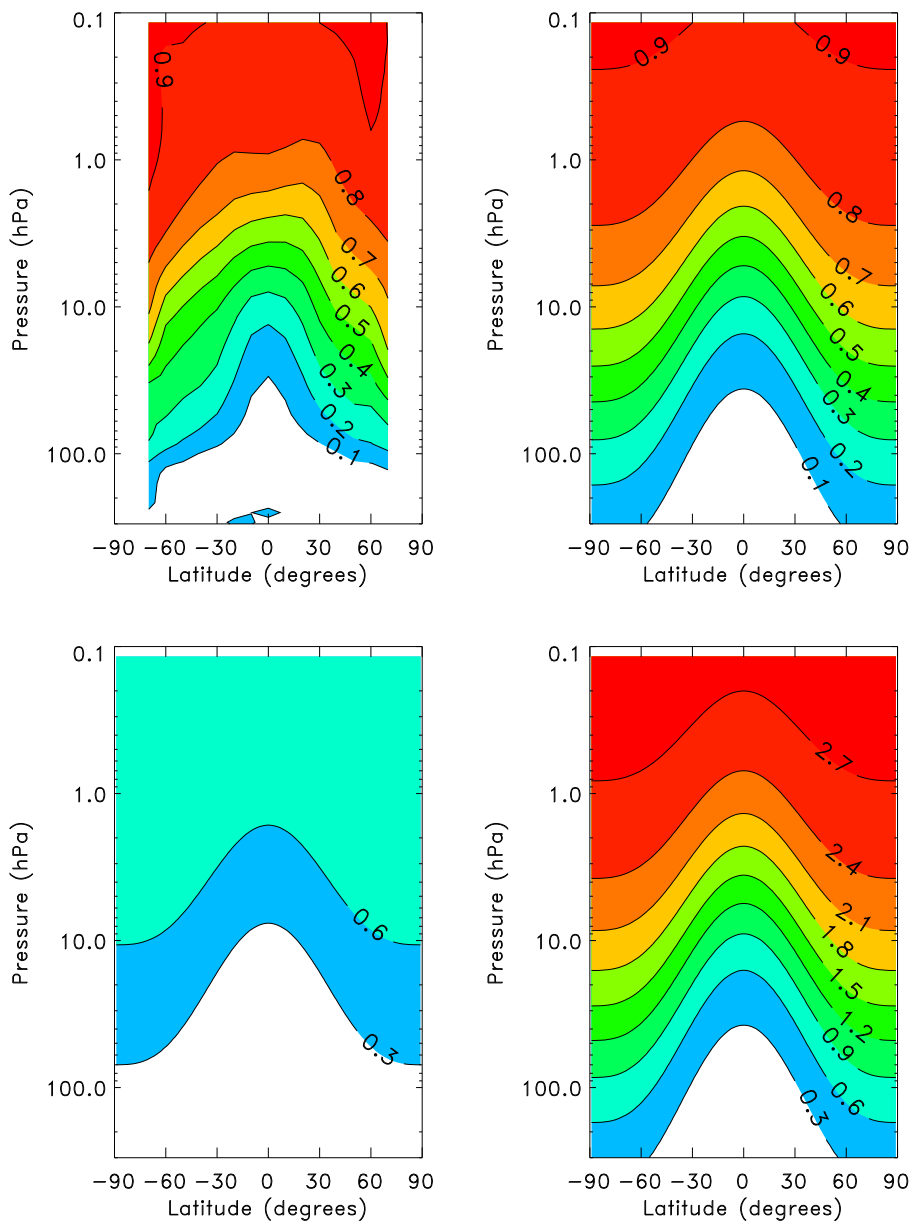


Figure 1



653

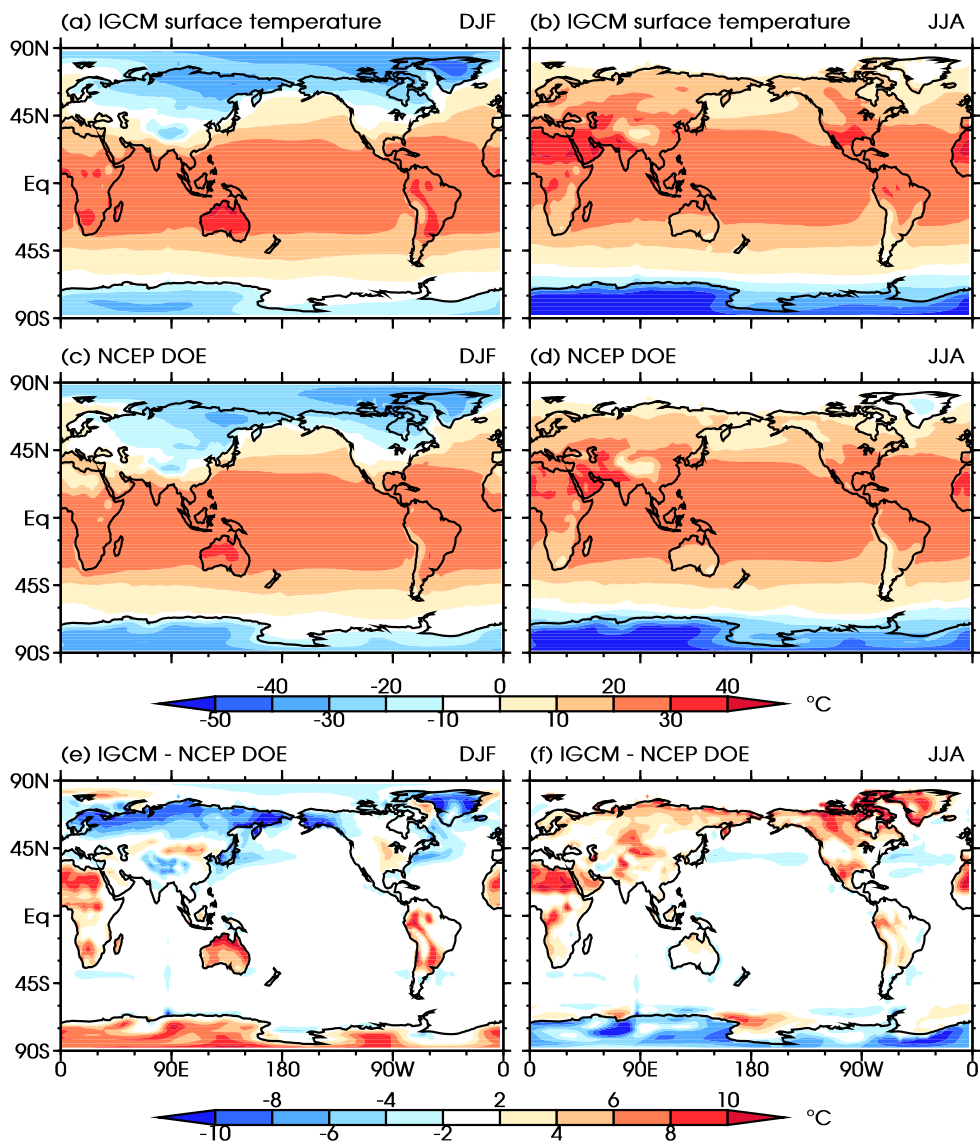
654

Figure 2

655

656

657



658

659

660

661

662

663

664

Figure 3

665  
666  
667  
668  
669  
670

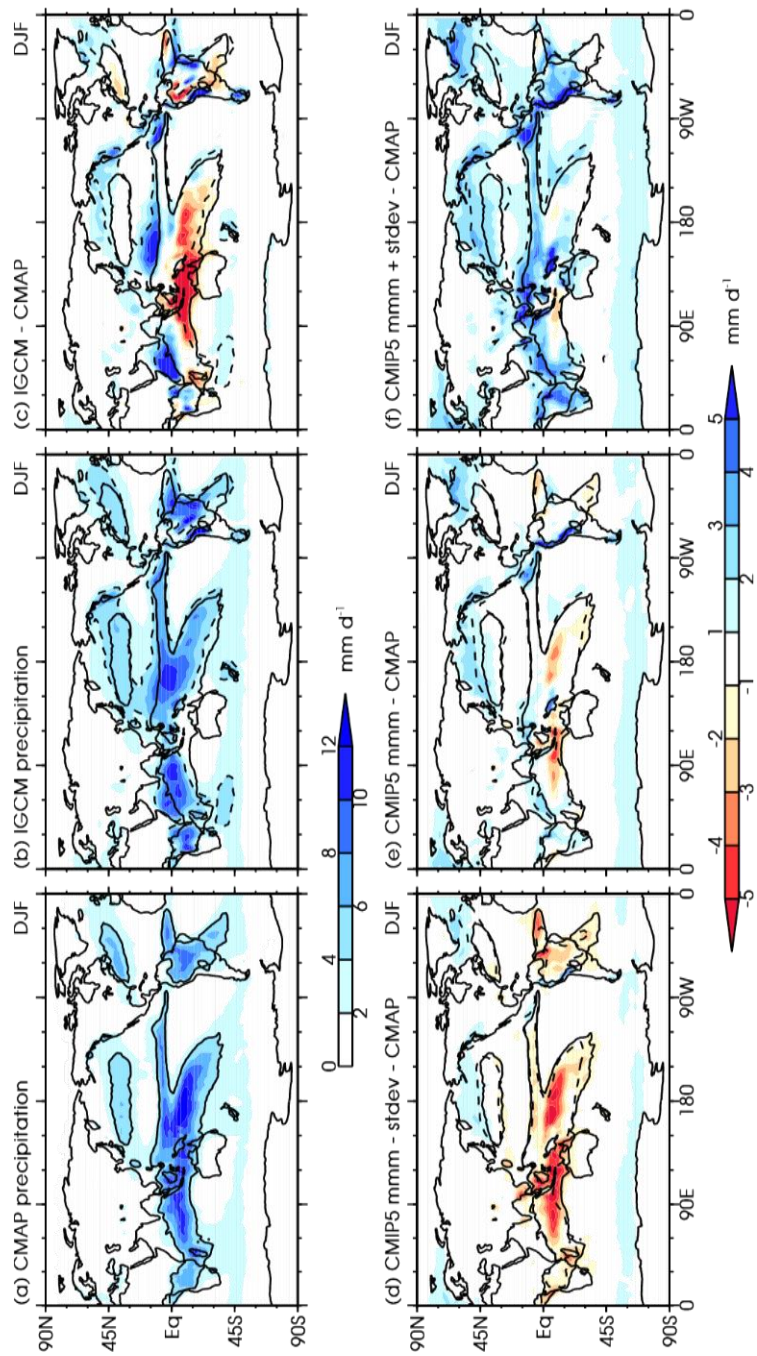
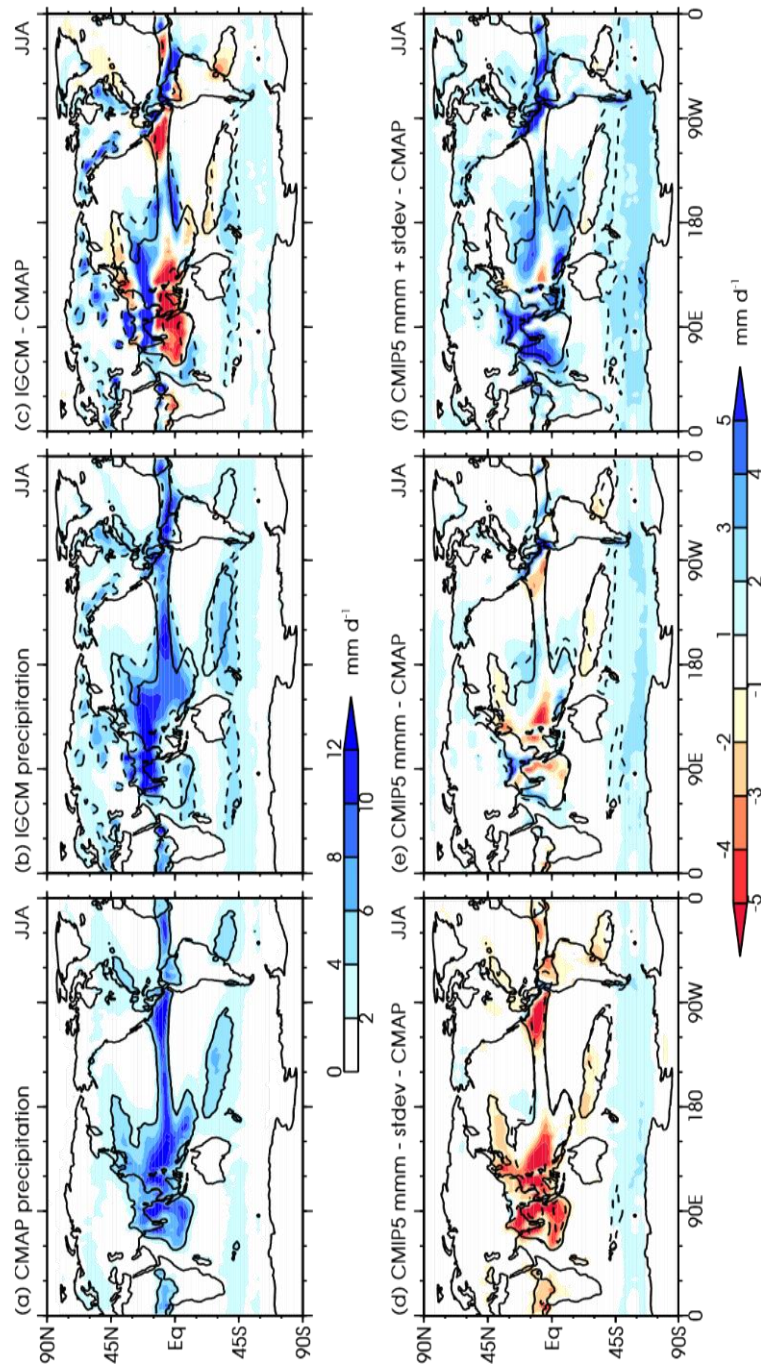


Figure 4



672

673

Figure 5

674

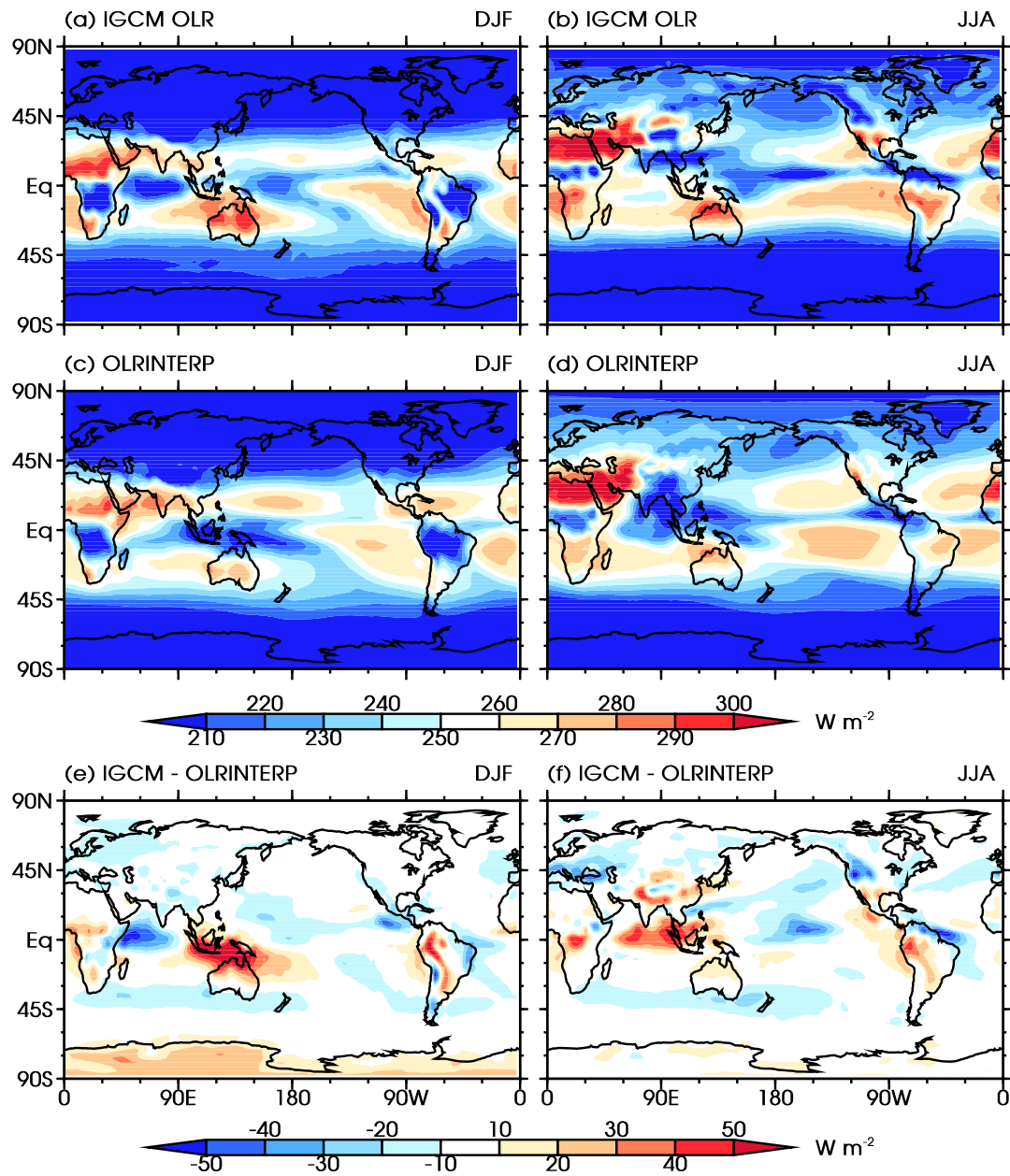
675

676

677

678

679



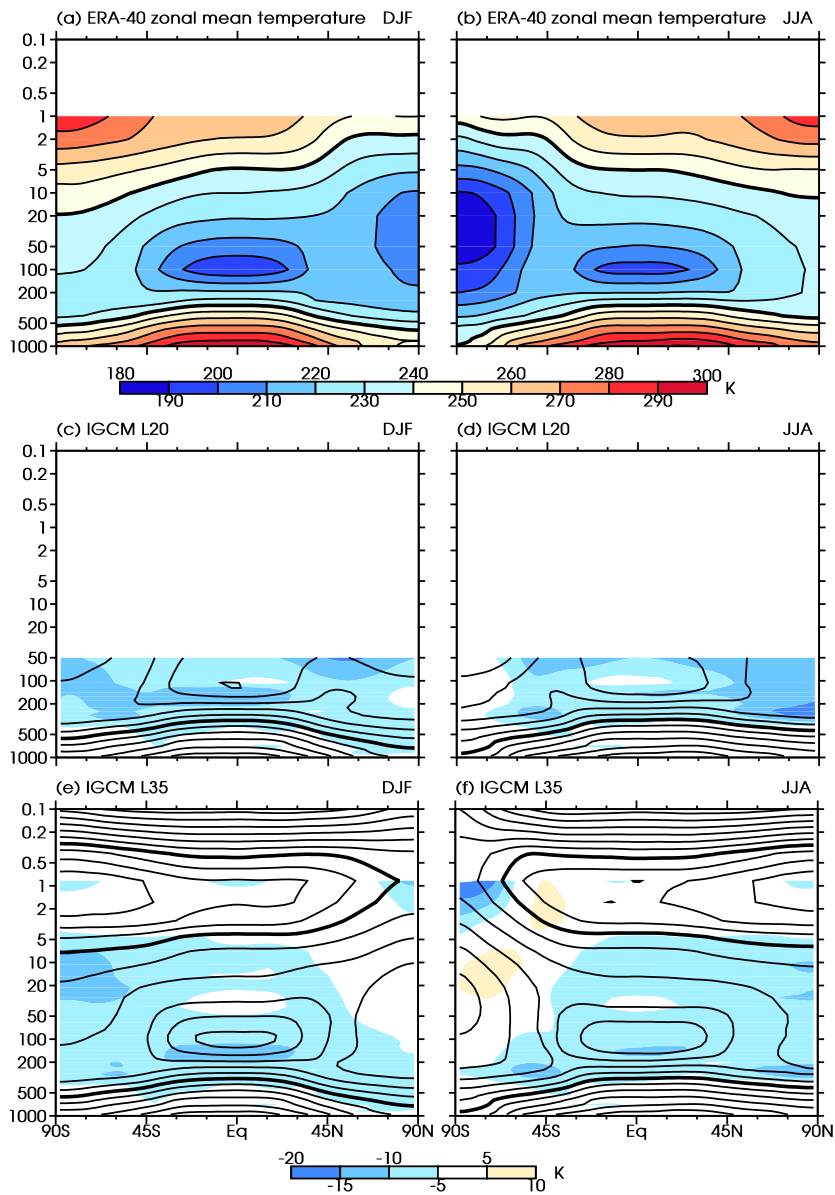
680

681

682

683

Figure 6



685

686

687

Figure 7

688

689

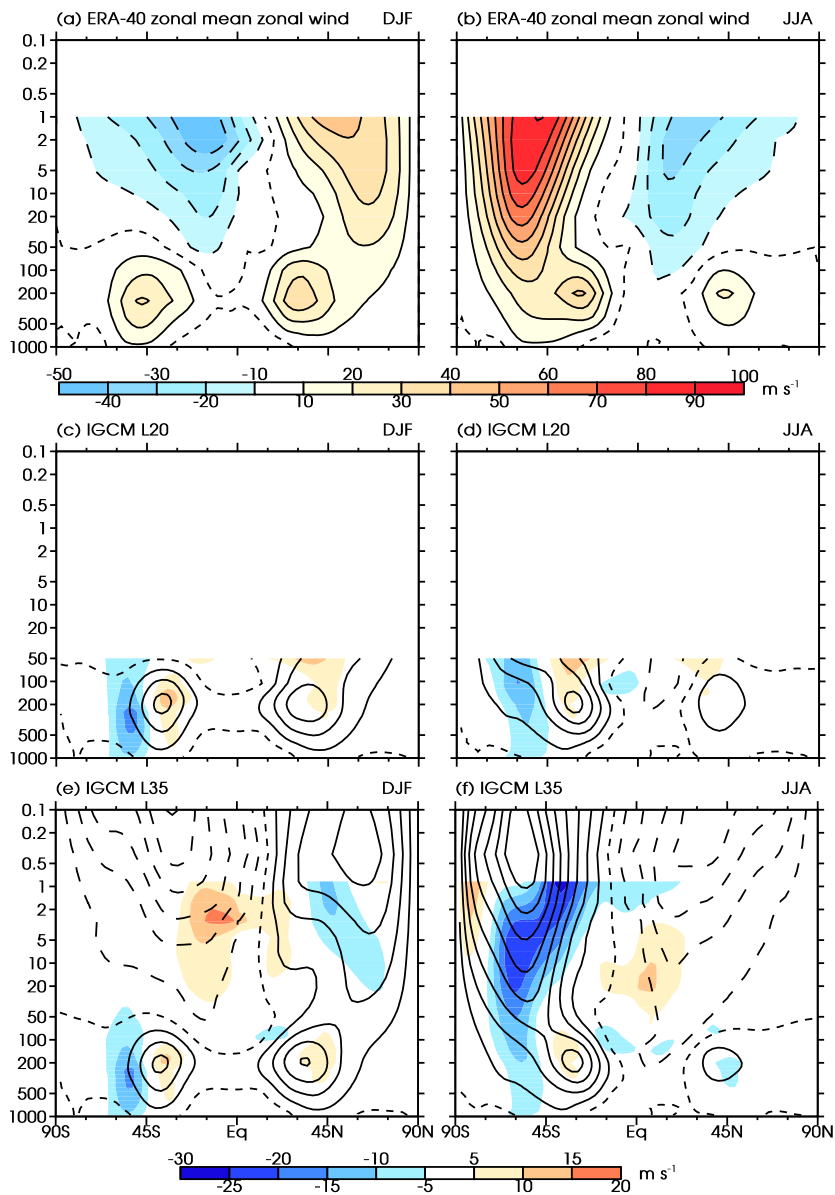
690

691



692

693



694

695

696

697

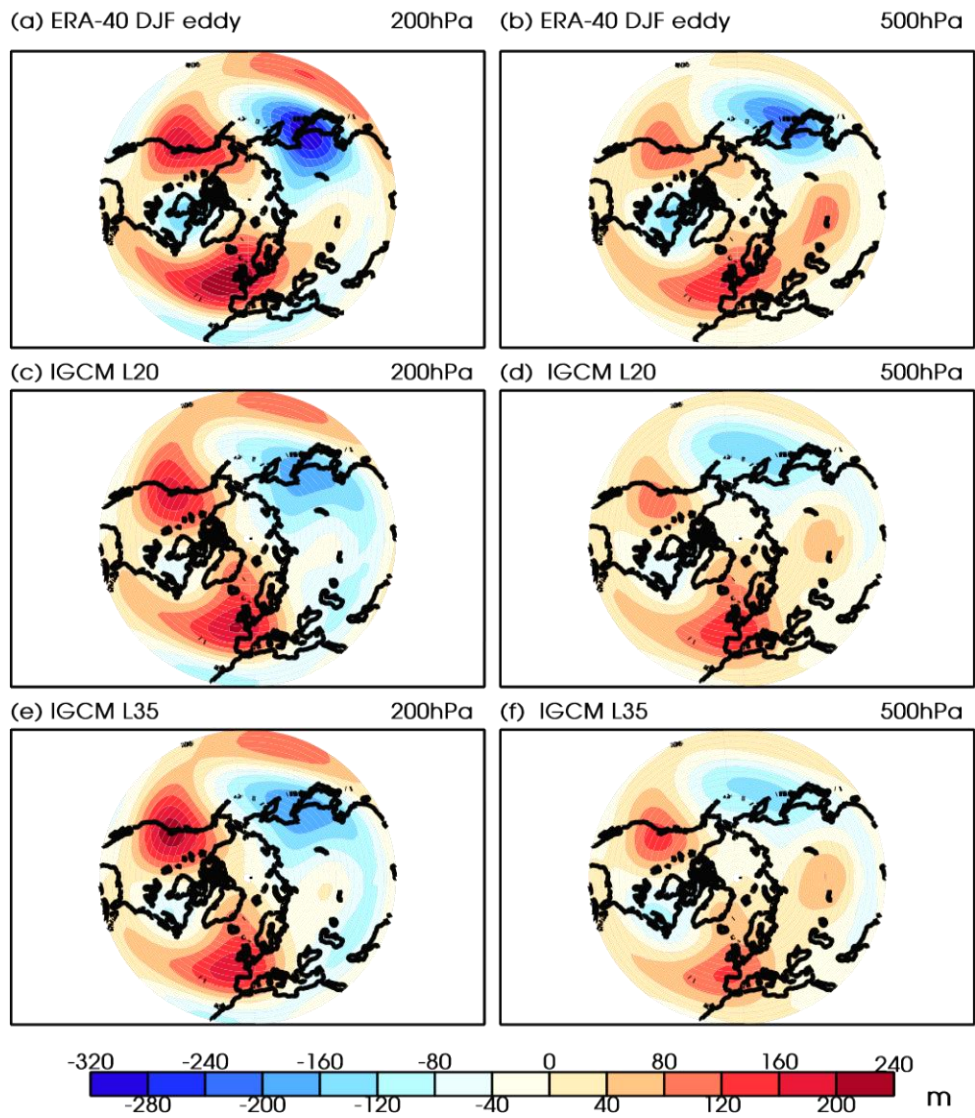
698

699

Figure 8

700

701

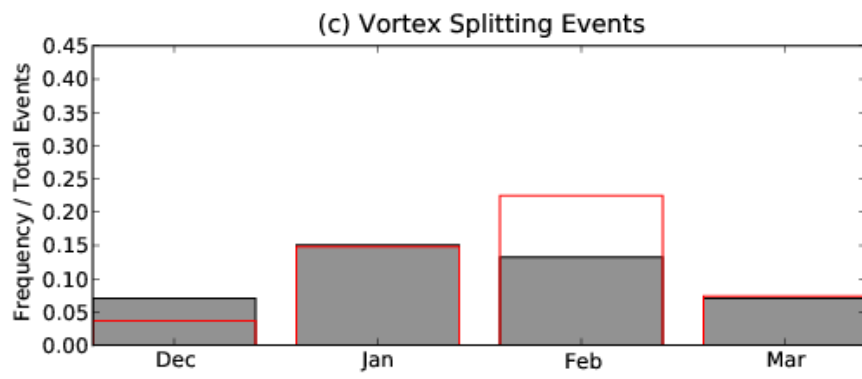
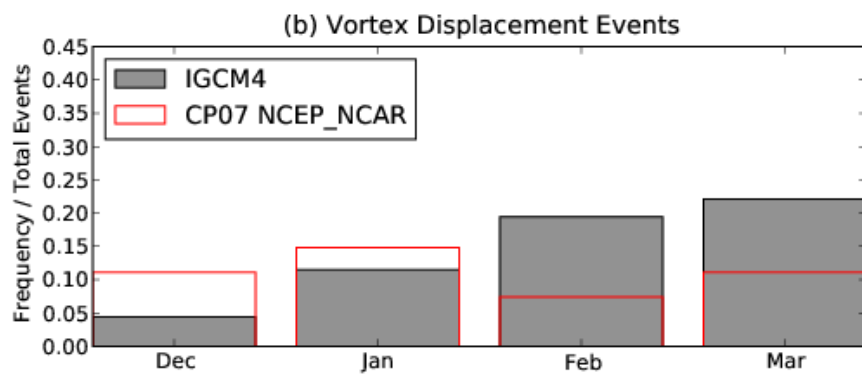
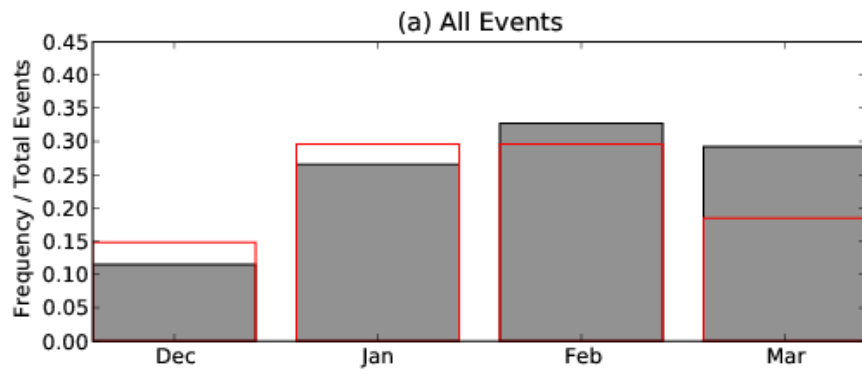


702

703

704

Figure 9



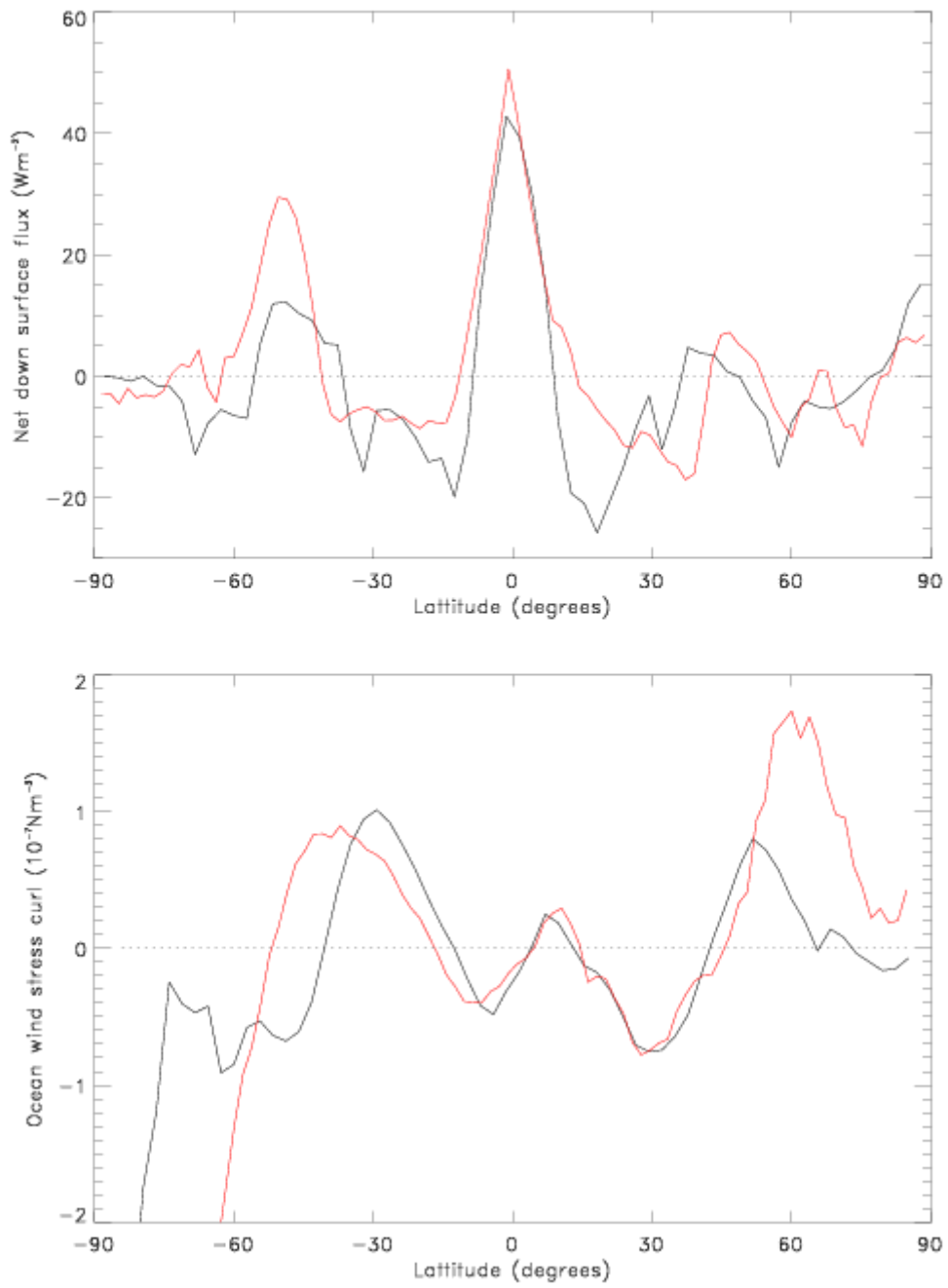
705

706

Figure 10

707

708



709

710

Figure 11